JACS
JOURNAL OF THE AMERICAN CHEMICAL SOCIETY
Article
pubs.acs.org/JACS

Photoinitiated Reactivity of a Thiolate-Ligated, Spin-Crossover Nonheme {FeNO}^{7} Complex with Dioxygen

Alison C. McQuilken,[†] Hirotoshi Matsumura,[‡,#] Maximilian Dürr,[§] Alex M. Confer,[†] John P. Sheckelton,[†,∥] Maxime A. Siegler,[†] Tyrel M. McQueen,[†,∥,⊥] Ivana Ivanović-Burmazović,*[,§] Pierre Moënne-Loccoz,*[,‡] and David P. Goldberg*[,†]

[†]Department of Chemistry, The Johns Hopkins University, Baltimore, Maryland 21218, United States
[‡]Oregon Health & Science University, Institute of Environmental Health, Portland, Oregon 97239, United States
[§]Department of Chemistry and Pharmacy, University of Erlangen-Nürnberg, 91058, Erlangen, Germany
[∥]Institute for Quantum Matter and Department of Physics and Astronomy, The Johns Hopkins University, Baltimore, Maryland 21218, United States
[⊥]Department of Materials Science and Engineering, The Johns Hopkins University, Baltimore, Maryland 21218, United States

Supporting Information

ABSTRACT: The nonheme iron complex, [Fe(NO)(N3PyS)]BF_4, is a rare example of an {FeNO}^{7} species that exhibits spin-crossover behavior. The comparison of X-ray crystallographic studies at low and high temperatures and variable-temperature magnetic susceptibility measurements show that a low-spin S = 1/2 ground state is populated at 0−150 K, while both low-spin S = 1/2 and high-spin S = 3/2 states are populated at T > 150 K. These results explain the observation of two N−O vibrational modes at 1737 and 1649 cm^{-1} in CD_3CN for [Fe(NO)(N3PyS)]BF_4 at room temperature. This {FeNO}^{7} complex reacts with dioxygen upon photoirradiation with visible light in acetonitrile to generate a thiolate-ligated, nonheme iron(III)-nitro complex, [$Fe^{III}(NO_2)$(N3PyS)]$^+$, which was characterized by EPR, FTIR, UV−vis, and CSI-MS. Isotope labeling studies, coupled with FTIR and CSI-MS, show that one O atom from O_2 is incorporated in the Fe^{III}−NO_2 product. The O_2 reactivity of [Fe(NO)(N3PyS)]BF_4 in methanol is dramatically different from CH_3CN, leading exclusively to sulfur-based oxidation, as opposed to NO· oxidation. A mechanism is proposed for the NO· oxidation reaction that involves formation of both Fe^{III}-superoxo and Fe^{III}-peroxynitrite intermediates and takes into account the experimental observations. The stability of the Fe^{III}-nitrite complex is limited, and decay of [$Fe^{III}(NO_2)$(N3PyS)]$^+$ leads to {FeNO}^{7} species and sulfur oxygenated products. This work demonstrates that a single mononuclear, thiolate-ligated nonheme {FeNO}^{7} complex can exhibit reactivity related to both nitric oxide dioxygenase (NOD) and nitrite reductase (NiR) activity. The presence of the thiolate donor is critical to both pathways, and mechanistic insights into these biologically relevant processes are presented.

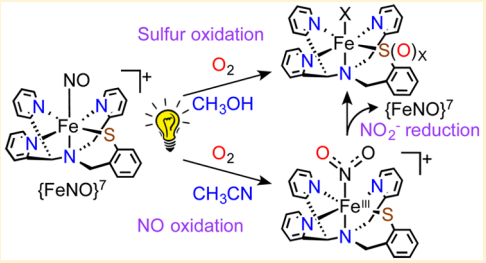

INTRODUCTION

Nitric oxide (NO·) is a well-known biological messenger responsible for such functions as vasodilation and neurotransmission, as well as immune response to bacterial infection.[1−4] NO· has a relatively short half-life and is metabolized to other nitrogen oxide derivatives (NO_x), i.e. nitrite (NO_2^-) and nitrate (NO_3^-), in the presence of O_2.[5−7] On the other hand, nitrite has been shown to be an important source of NO·.[8−13] For example, nitrite reductase (NiR) activity is believed to occur with ferriheme proteins hemoglobin (Hb) and myoglobin (Mb) in mammalian blood and tissue to invoke vasodilation by release of NO· (Hb + NO_2^- + 2 H^+ → metHb + NO· + H_2O).[14−16] In general, metals have been shown to play an important role in the interconversion between NO· and NO_2^-.[17,18] Synthetic examples have been reported for the generation of iron−nitrite complexes from the aerobic oxidation of iron nitrosyls or by inner-sphere electron transfer between μ-oxo heme-Fe^{III}−O−Cu^{II}(L) complexes and NO·.[19−24] In some cases, this reaction is reversible upon oxygen atom transfer from Fe−NO_2^- to an external substrate to regenerate the Fe−NO complex ($Fe^{III}(NO_2^-)$ + S → Fe^{II}(NO) + SO).[5,19−21,25,26] The binding mode and H-bonding interactions of the Fe−NO_2^- species, together with the source of the reducing substrate, are important variables that need to be examined.[27,28]

While NO· has been characterized as an important signaling molecule in biology, it has also been implicated in the deleterious production of reactive oxidation products, such as nitrogen dioxide (NO_2·) and peroxynitrite ($OONO^-$).[29,30] Metal-peroxynitrite species are short-lived and either isomerize to give metal-nitrate species (M-NO_3^-) or decay to give metal-nitrite species (M−NO_2^-).[17,31] M−$OONO^-$ intermediates have been proposed for many enzymatic and model complexes

Received: December 7, 2015
Published: February 26, 2016

DOI: 10.1021/jacs.5b12741
J. Am. Chem. Soc. 2016, 138, 3107−3117

that contain metals such as Cu, Co, Fe, Cr, Rh, and Re. M−OONO$^-$ species have been suggested to form as transient intermediates from either metal-superoxo (M−OO$^-$) + NO· or from M−NO + O_2, eventually yielding M−NO_3^- and M−NO_2^- species.[17,32−41] For example, Hb-O_2 and Mb-O_2 react with NO· to give NO_3^-, which is described as nitric oxide dioxygenase (NOD) reactivity.

Previous work on synthetic nonheme iron nitrosyl complexes has provided insight into the properties of these {FeNO}^{7} species,[42,43] but there is still a need for understanding their reactivity in critical oxidative and reductive pathways. There are some biomimetic studies using these synthetic {FeNO}$^{7/8}$ complexes focused on NO· reduction to N_2O[44−48] and generation of nonheme {FeNO}^{7} complexes by reduction of nitrite (i.e., nitrite reductase (NiR) activity).[19,21,49] Less is known, however, about the role of nonheme iron centers in NO· oxidation (e.g., NOD reactivity).[20,29,39−41,50−55]

Previous work from our lab has focused on determining the reactivity of nonheme iron complexes with dioxygen. A recent focus concerned the construction of synthetic analogs of cysteine dioxygenase (CDO),[56−63] a mononuclear nonheme Fe enzyme that converts cysteine to cysteine sulfinic acid with O_2.[64,65] Evidence indicates that the substrate cysteine must bind to the Fe center in CDO prior to O_2 activation, and we showed that incorporation of a thiolate donor in a synthetic analog of CDO was required for O_2 reactivity. Through ligand design and the synthesis of a series of Fe complexes, it was determined that biologically relevant thiolate-to-sulfinate S-oxygenation occurs with the nonheme Fe complex [Fe^{II}(N3PyS)(CH_3CN)]BF_4 (**1**), in which a facial disposition of pyridine N donors is incorporated, similar to the unusual His triad in CDO.[62] A likely mechanism for S-oxygenation involved an Fe^{III}-superoxo intermediate generated from **1** + O_2. Although this intermediate was not directly observed, nitric oxide was employed as an O_2 surrogate and gave a structurally characterized {FeNO}^{7} complex with NO· bound in the proposed O_2 binding site of **1**.[63] These findings, along with the realization that little is known about nonheme iron-nitrosyl reactivity with dioxygen, directed our efforts toward studying the O_2 reactivity of this {FeNO}^{7} complex.

The syntheses of [Fe^{II}(N3PyS)(CH_3CN)]BF_4 (**1**)[62] and its corresponding {FeNO}^{7} complex, [Fe(NO)(N3PyS)]BF_4 (**2**),[63] were previously reported, and the photolytic release of NO· upon irradiation with visible light (λ > 400 nm) was demonstrated. An all-nitrogen ligated analog, [Fe(NO)(N4Py)]BF_4 (**3**), was also prepared but showed no release of NO· upon photoirradiation. These {FeNO}^{7} complexes are shown in Figure 1. The electronic configuration of the low-spin (S = 1/2) complex **2** was determined via EPR, Mössbauer, XAS, and DFT calculations to be low-spin Fe^{II} (S = 0) coupled to NO· (S = 1/2) with some mixing of low-spin Fe^{III} (S = 1/2) coupled to NO$^-$ (S = 0). The ATR-IR spectrum of **2** unexpectedly showed two bands in the region typical for N−O stretches (ν(NO)) for six-coordinate {FeNO}^{7} complexes, and both were shifted upon isotopic substitution. A linear correlation between Fe−N−O bond angle and ν(NO) for six-coordinate {FeNO}^{7} species was described,[66] and a factor that can contribute to this correlation is the spin state of the {FeNO}^{7} complex, with high-spin (S = 3/2) species typically exhibiting higher frequency N−O stretches and low-spin (S = 1/2) species exhibiting lower frequency modes.

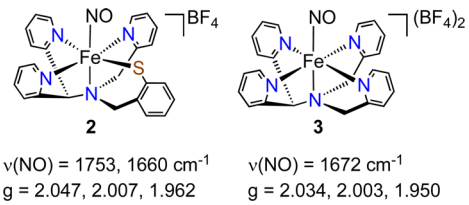

Figure 1. [Fe(NO)(N3PyS)]BF_4 (**2**) and [Fe(NO)(N4Py)]$(BF_4)_2$ (**3**) with vibrational and EPR data.

In this work, low-temperature IR spectroscopy, magnetic susceptibility measurements, and a comparison of low- and high-temperature single crystal X-ray diffraction (XRD) analyses were employed to determine the origin of the two vibrational bands seen for **2**. These data show that the two vibrational modes result from gradual spin-crossover behavior, which classifies **2** as a rare example of a six-coordinate {FeNO}^{7} complex that exhibits spin-crossover.[24,67]

The reactivity of **2** with O_2 is also presented. The proposed mechanism for S-oxygenation of **1** relied upon an Fe^{III}-superoxo complex, and we hypothesized that photorelease of NO· from **2** in the presence of O_2 might provide controlled access to an $Fe^{III}(O_2^-)$ species. Upon photoirradiation with visible light, complex **2** reacts with O_2 to give an Fe^{III}−nitrite complex. Spectroscopic methods (IR, UV−vis), isotope labeling (^{18}O), and high-resolution, low-temperature electrospray mass spectrometry are used to follow the O_2 reactivity, showing the formation and decay (via nitrite reduction) of the Fe^{III}−nitrite complex. Thus, this work provides a novel method for accessing nonheme Fe^{II}/O_2 reactivity involving photorelease of NO·, and also demonstrates that a thiolate-ligated nonheme Fe complex can mediate both NO· oxidation and nitrite reduction chemistry. A mechanism is suggested that involves a common Fe^{III}-superoxo intermediate that branches toward either NO· or S-oxygenation chemistry depending upon reaction conditions. These findings can be compared to enzymatic nitric oxide dioxygenase and nitrite reductase reactivity.

EXPERIMENTAL METHODS

General Procedures. All reagents were purchased from commercial vendors and used without further purification unless otherwise noted. Dichloromethane was purified via a Pure-Solv Solvent Purification System from Innovative Technology, Inc. Methanol and acetonitrile were distilled over CaH_2. All solvents were degassed by repeated cycles of freeze−pump−thaw and stored in an N_2-filled drybox. Nitric oxide gas was purchased from Matheson gases and purified according to a literature procedure[68] and was stored in a sealed Schlenk flask until use. ^{15}NO (>98% ^{15}N) and $^{15}N^{18}O$ (>98% ^{15}N, > 95% ^{18}O) gases were purchased from Cambridge Isotope Laboratory and Isotec, respectively. The iron(II) starting material, [Fe^{II}(N3PyS)(CH_3CN)]BF_4 (**1**),[62] and the {FeNO}^{7} starting material, [Fe(NO)(N3PyS)]BF_4 (**2**),[63] were synthesized according to literature procedures.

Physical Methods. UV−visible spectra were recorded on a Hewlett-Packard 8542 photodiode-array spectrophotometer equipped with HPChemstation software or on a Varian Cary 50 Bio spectrophotometer. ^1H spectra were recorded on a Bruker Avance 400 MHz FT-NMR spectrometer at 25 °C. Electron paramagnetic resonance (EPR) spectroscopy was performed on a Bruker EMX spectrometer controlled with a Bruker ER 041 X G microwave bridge and equipped with a continuous-flow liquid helium cryostat (ESR900) coupled to an Oxford Instruments TC503 temperature controller. The spectra were obtained at 12 K under nonsaturating microwave power conditions (ν = 9.475 GHz, microwave power = 0.201 mW, modulation amplitude = 10 G, modulation frequency = 100 kHz).

DOI: 10.1021/jacs.5b12741
J. Am. Chem. Soc. 2016, 138, 3107−3117

Cryospray ionization mass spectrometry (CSI-MS) was performed on a UHR-TOF Bruker Daltonik (Bremen, Germany) maXis 5G, an ESI-quadrupole time-of-flight (qToF) mass spectrometer capable of resolution of at least 60 000 FWHM. Detection was in positive-ion mode, and the source voltage was 3.2 kV. The flow rates were 250 μL/h. The drying gas (N_2), to aid solvent removal, was held at −35 °C, and the spray gas was held at −40 °C. Energy-resolved collision-induced dissociations (MS2, CID) were conducted in a collision cell following a mass selecting quadrupole and preceding the high resolution daughter ion analysis in the TOF analyzer. Nitrogen (N_2) served as the collision gas. The machine was calibrated prior to every experiment via direct infusion of the Agilent ESI-TOF low concentration tuning mixture, which provided an m/z range of singly charged peaks up to 2700 Da in both ion modes. Magnetization was measured from T = 2 to 320 K on a powder sample of **2** using a Quantum Design Physical Properties Measurement System (PPMS) under an applied field of $\mu_0 H$ = 1 T.

Photoirradiation of [Fe(NO)(N3PyS)]BF_4 (2) in the Presence of O_2. A solution of **2** (2 mL, 0.2 mM) in CH_3CN was loaded into a quartz cuvette (1 cm path length) under N_2 and sealed with a rubber septum. The cuvette was clamped inside the UV−vis spectrophotometer such that spectra could be collected during the photoirradiation experiment. A halogen lamp (150 W) was positioned at a distance of 12 cm from the quartz cuvette ∼90° to the UV−vis beam, with a 400 nm long-pass filter placed between the cuvette and the lamp. The septum was removed to expose the solution to air, and the photoirradiation was initiated and maintained for 10 min. An initial color change from brown to red was observed, with bands between 400 and 500 nm (0−60 s). These features then decayed with concomitant growth of the 840 nm band, assigned to $[Fe^{III}(NO_2)(N3PyS)]^+$ (**4**). The reaction was monitored by EPR spectroscopy following a similar procedure, wherein a solution of **2** (0.8 mL, 1.15 mM) in toluene/CH_3CN was positioned ∼6 cm from a halogen lamp (150 W) with a 400 nm long-pass filter placed between the lamp and the cuvette. The solution in the cuvette was exposed to air, and photoirradiation was carried out for 12−13 min, with monitoring by UV−vis to confirm the complete formation of the 840 nm band. An aliquot (400 μL) was loaded into an EPR tube and frozen in LN_2 via slow annealing for storage at 77 K until further use.

Analytical Quantification of Nitrite Ion. A solution of [Fe(NO)(N3PyS)]BF_4 (**2**) (2 mL, 0.7 mM) in CH_2Cl_2 was loaded into a quartz cuvette (1 cm path length) and sealed with a rubber septum under N_2. The cuvette was clamped inside the UV−vis spectrophotometer such that spectra could be collected during the photoirradiation experiment. A halogen lamp (150 W) was positioned at a distance of 12 cm from the quartz cuvette ∼90° to the UV−vis beam, with a 400 nm long-pass filter placed between the cuvette and the lamp. The septum was removed to expose the solution to air, and the photoirradiation was initiated and maintained for 10 min. The growth of the feature at 800 nm, corresponding to the generation of $[Fe^{III}(NO_2)(N3PyS)]^+$ in CH_2Cl_2, was observed. This solution was then vigorously stirred with an aqueous solution of NaCl (1 mM, 2 mL) for 5 min to extract nitrite into the aqueous layer. The yield of nitrite was determined by using QUANTOFIX Nitrite semi-quantitative test strips (MACHEREY-NAGEL, Germany) by color comparison with known concentrations of nitrite in solution. The amount of nitrite extracted into the aqueous layer was estimated to give a 33% yield.

Transmittance FTIR Measurements. FTIR films were prepared by loading CaF_2 cells equipped with 25 μm spacers with 20 μL of complex **2** at 2 mM in CD_3CN (anaerobic or saturated with O_2). For all samples, the presence of the NO· adduct was confirmed by UV−vis spectroscopy. For low-temperature FTIR, the cell was mounted to a sample rod and frozen in liquid nitrogen before insertion in a closed-cycle cryostat (Omniplex, Advanced Research System). Irradiation of the FTIR films was performed with the 514 nm line of an argon laser (Innova 90, Coherent). The laser power was set at 100 mW and defocused to a 1 cm diameter beam in order to illuminate the entire FTIR film. FTIR spectra were collected with a Bruker Tensor 27 equipped with a liquid nitrogen-cooled MCT detector using sets of 100 scan accumulations acquired at 4 cm^{-1} resolution. Multiple FTIR spectra were first collected in the dark, before collecting spectra under illumination ("light" spectra for complex **2** in anaerobic CD_3CN at room temperature) or after illumination ("illuminated" spectra). Illumination of complex **2** in O_2-saturated CD_3CN at room temperature was limited to 10 s immediately prior to collecting "illuminated" spectra. Consecutive accumulations of 100-scan spectra requiring a 45-s acquisition time showed no evidence of precursor species to the nitrite product of the photoreaction. FTIR spectra obtained several minutes after the 10-s illumination showed a gradual decrease of the $\nu(NO_2)$ modes consistent with thermal instability of the nitrite product at high concentration.

Chemical Oxidation of [Fe^{II}(N3PyS)(CH_3CN)]BF_4 (1) and Addition of Bu_4NNO_2. A solution of **1** (2 mL, 0.2 mM) in CH_3CN was loaded into a quartz cuvette (1 cm path length) and sealed with a rubber septum. Under Ar, 1 equiv of $FcPF_6$ was added (50 μL, 8 mM in CH_3CN), and the red solution immediately turned brown-green, with a λ_{max} = 880 nm ($\varepsilon \approx 1400$ M^{-1} cm^{-1}). Subsequent addition of 1 equiv of Bu_4NNO_2 (25 μL, 16 mM in CH_3CN) caused a further color change to brown with a new λ_{max} = 840 nm. This spectrum matched that from the aerobic photoirradiation of $[Fe(NO)(N3PyS)]^+$. The reaction was monitored by EPR spectroscopy following a similar procedure. To a solution of **1** (350 μL, 2.2 mM) in toluene/CH_3CN in an N_2-filled drybox was added 1 equiv $FcPF_6$ (45 μL, 16.5 mM), and an immediate color change to brown-green was observed. This solution was stirred for 30 s, then 1 equiv Bu_4NNO_2 (40 μL, 18 mM) was added, resulting in another color change to brown. An aliquot (400 μL) was immediately transferred to an EPR tube, taken out of the drybox, and frozen in LN_2 via slow annealing.

Photoirradiation of [Fe(NO)(N3PyS)]BF_4 (2) in Methanol. A solution of **2** (2 mL, 0.2 mM) in CH_3OH was loaded into a quartz cuvette (1 cm path length) under N_2 and sealed with a rubber septum. The cuvette was clamped inside the UV−vis spectrophotometer such that spectra could be collected during the photoirradiation experiment. A halogen lamp (150 W) was positioned at a distance of 12 cm from the quartz cuvette ∼90° to the UV−vis beam, with a 400 nm long-pass filter placed between the cuvette and the lamp. The photoirradiation was initiated and maintained for 25 min. Conversion to the UV−vis spectrum corresponding to $[Fe^{II}(N3PyS)(solv)]BF_4$ in methanol (λ = 450, 530 nm) was observed. Once the photorelease of NO· from **2** was complete, the halogen lamp was switched off and rebinding of NO· was observed by UV−vis over 4 h. The aerobic photoirradiation experiment was done under similar conditions, except the septum was removed to expose the solution to air and the photoirradiation was initiated and maintained for 30 min, with full conversion to the green species (λ_{max} = 674 nm).

Cryospray Ionization Mass Spectrometry (CSI-MS). In a typical experiment, an amount of **2** (5 mg, 9 μmol) was dissolved in a vial in CH_3CN or CH_3OH (5 mL, HPLC Ultra Gradient grade) in the drybox. CSI-MS was measured for $[Fe(NO)(N3PyS)]^+$ prior to photoirradiation and air exposure. The vial was then exposed to air, and the solution was irradiated with a 150 W xenon lamp using a 30 mm TLC-chamber filled with water as a UV-filter. CSI-MS measurements were carried out after 5, 10, and 20 min of irradiation.

CSI-MS analysis for the $^{18}O_2$ labeling study was prepared by generating an 8.1 mM solution of $^{18}O_2$ in CH_3CN (produced via freeze−pump−thaw). An amount of **2** (1.2 mg, 2 μmol) was dissolved in 40 mL of CH_3CN. CSI-MS was measured for $[Fe(NO)(N3PyS)]^+$ prior to photoirradiation and addition of $^{18}O_2$. Next, 1.5 equiv (260 μL) of the $^{18}O_2$ solution was added to **2**, and the solution was irradiated under the same conditions as previously discussed. CSI-MS measurements were carried out after 1, 5, 10, and 25 min of irradiation.

CSI-MS analysis for the chemical oxidation of **1** and addition of Bu_4NNO_2 was prepared by dissolution of **1** in CH_3CN (1.2 mg, 40 mL). Equimolar amounts of $FcBF_4$ and Bu_4NNO_2 were added in succession, and the CSI-MS was measured after each addition.

DOI: 10.1021/jacs.5b12741
J. Am. Chem. Soc. 2016, 138, 3107−3117

RESULTS AND DISCUSSION

Temperature Dependence of Structural Parameters for [Fe(NO)(N3PyS)]BF_4 (2). The crystal structure of **2** was previously reported at 110(2) K.[63] To determine if two spin states exist at higher temperature, which would support the presence of two N−O stretching bands, data for **2** were recollected at 293(2) K. As seen in Table 1, there is a significant elongation in all Fe−N_{ligand} bond lengths for the high temperature structure at 293 K as compared to the low-temperature structure at 110 K. There is very slight lengthening of the Fe−S bond distance (~0.02 Å), which is not surprising given that other Fe−S bond distances of thiolate-ligated S = 3/2 {FeNO}^{7} complexes are similar.[22,69] This elongation is indicative of a significant population of the high-spin (S = 3/2) state for this {FeNO}^{7} complex. These findings help to explain the observation of the two N−O vibrational modes and are in good agreement with variable-temperature magnetic susceptibility data collected for **2** (vide infra).

Table 1. Comparison of Selected Bond Distances (Å) for [Fe(NO)(N3PyS)]BF_4 (2) Determined at 110(2) K and 293(3) K[a]

	110 K	293 K
Fe−N1	2.1300(16)	2.188(2)
Fe−$N2_{py}$	1.9909(17)	2.107(3)
Fe−$N3_{py}$	2.0297(16)	2.147(2)
Fe−$N4_{py}$	2.0085(17)	2.074(3)
Fe−S1	2.2962(5)	2.3156(9)
Fe−N5(O)	1.7327(18)	1.747(3)

[a]See Figure S1 for atom label assignments and structures.

Magnetism. The temperature dependent magnetic susceptibility data ($\chi_m \cdot T$ vs T, corrected for temperature independent contribution to the susceptibility, χ_0) are shown in Figure 2. In a purely paramagnetic, noninteracting system with no spin transitions, $\chi_m \cdot T$ vs T should be a constant value over all temperatures equal to the Curie constant, and the dashed lines indicate the expected values for purely S = 1/2 and S = 3/2 species. The region from 10−150 K is effectively constant at the value of C extracted from the inverse susceptibility, which is close to the spin-only value of an S = 1/2 system. However, at values of T > 150 K, $\chi_m \cdot T$ continually increases all the way up to the highest temperature measured, T = 320 K. These data confirm that **2** exhibits a low-spin (S = 1/2) state at low temperature, with an increasing contribution from a high-spin (S = 3/2) state as the temperature is increased above $T \approx 150$ K. Modeling the data assuming two spin states separated by an energy difference (Δ) yields 20% in the high spin state at T = 300 K and an energy gap between the states of Δ = 500 K. This agrees well with an estimate of 25% in the high spin state at T = 320 K obtained by applying a lever rule to the observed net Curie constant at that temperature.

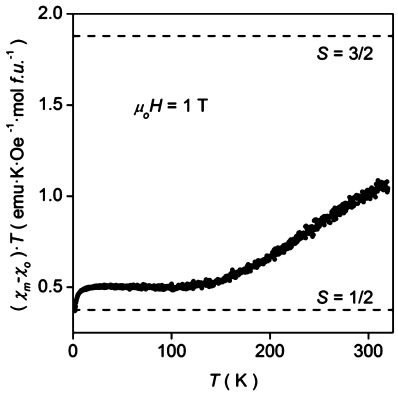

Figure 2. Magnetic susceptibility data of **2** as a function of temperature.

Temperature-Dependent Infrared Spectroscopy of 2. Previous ATR-IR spectra of crystalline **2** showed two bands at 1753 and 1660 cm^{-1} that shift upon $^{15}N^{18}O$ labeling to 1677 and 1587 cm^{-1}, respectively. In CD_3CN, these bands were also observed at 1733 and 1649 cm^{-1}, but the band at 1733 cm^{-1} was much less intense. Upon addition of isotopically labeled $^{15}N^{18}O$, a shift in the band at 1649 cm^{-1} was observed (1582 cm^{-1}), but the other band ($\nu(NO)_{calc}$ = 1655 cm^{-1}) was too weak to detect.[63] Transmittance FTIR spectra of complex **2** in CD_3CN are dominated by solvent vibrations, but ν(NO) modes of complex **2** can be extracted from these spectra by taking advantage of the photolabile character of the nitrosyl complex. Despite fast rebinding kinetics of NO· at room temperature, illuminating IR films inside the sample chamber with white light during spectral acquisition can lead to a sufficient population of dissociated species, and differences between spectra obtained in the dark and under illumination (i.e., "dark" minus "light") isolate ν(NO) modes at 1737 and 1649 cm^{-1} that shift to lower frequency with ^{15}NO· and $^{15}N^{18}O$· (Figure 3). Specifically, complex **2** prepared with ^{15}NO· displays ν(NO) bands at 1705 and 1618 cm^{-1} while labeling with $^{15}N^{18}O$ results in a further downshift to 1661 and 1582 cm^{-1}, respectively, with evidence of Fermi coupling of the 1582 cm^{-1} mode with N3PyS ligand vibrations. All observed isotopic shifts are within a few wavenumbers of expected values calculated for harmonic diatomic oscillators.

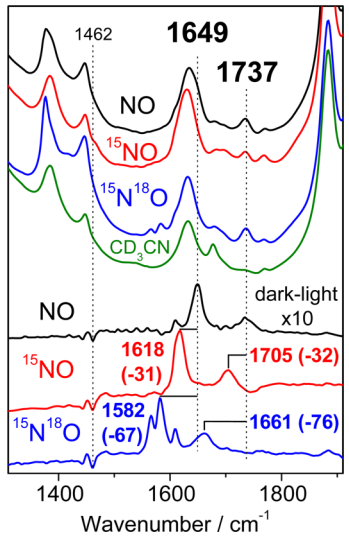

Figure 3. Room-temperature FTIR spectra of **2** in CD_3CN (top three traces: unlabeled NO· (black), ^{15}NO· (red), and $^{15}N^{18}O$· (blue); the spectrum of the neat solvent is also shown in green for comparison), and "dark" minus "light" difference spectra (bottom three traces: unlabeled NO· (black), ^{15}NO· (red), and $^{15}N^{18}O$· (blue); the difference spectra were multiplied by a factor 10 to facilitate comparison with the raw spectra).

DOI: 10.1021/jacs.5b12741
J. Am. Chem. Soc. 2016, 138, 3107−3117

Light-induced FTIR difference spectra were also obtained on complex **2** dissolved in CD_3CN and maintained at 15 K. At cryogenic temperatures, the caging effect of the frozen solvent limits the efficiency of the photodissociation process, but at sufficiently low temperature, it can also prevent geminate rebinding of NO· to lead to trapping of a small population of the dissociated state after the illumination is turned off. Accordingly, "dark" minus "illuminated" difference spectra reveal a single ν(NO) mode at 1641 cm^{-1}, which is consistent with a low-spin {FeNO}^{7} species that shifts to 1612 cm^{-1} with ^{15}NO·. As expected, the ν(NO) is further downshifted with $^{15}N^{18}O$ and split into two bands at 1561 and 1579 cm^{-1} through coupling with an N3PyS ligand vibration (Figure 4).

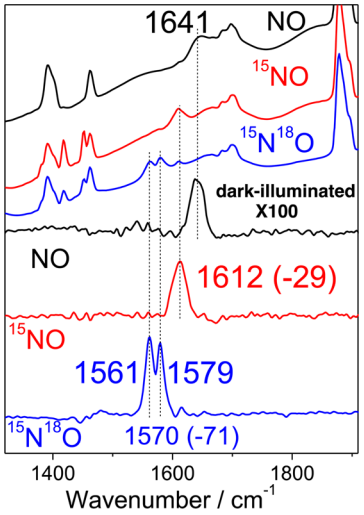

Figure 4. FTIR spectrum of **2** in CD_3CN at 15 K (top three traces: unlabeled NO· (black), ^{15}NO· (red), and $^{15}N^{18}O$· (blue)), and "dark" minus "illuminated" difference spectra (bottom three traces: unlabeled NO· (black), ^{15}NO· (red), and $^{15}N^{18}O$· (blue); the difference spectra were multiplied by a factor 100 to facilitate comparison with the raw spectra).

Thus, the FTIR data support the X-ray crystallography and magnetic susceptibility studies in showing that complex **2** exists in a temperature-dependent high-spin (S = 3/2) and low-spin (S = 1/2) equilibrium with distinct N−O stretching frequencies. Taken together, these results show that **2** is a rare example of a six-coordinate {FeNO}^{7} complex that exhibits spin-crossover behavior. This spin equilibrium is in fact more likely due to valence tautomerism between a high-spin (S = 5/2) Fe^{III} antiferromagnetically coupled to NO^- (S = 1) and a low-spin (S = 0) Fe^{II} coupled to NO· (S = 1/2).[67]

Reactivity of {FeNO}^{7} Complexes with O_2. Visible light irradiation of $[Fe(NO)(N3PyS)]BF_4$ (**2**) with a halogen lamp and 400 nm long-pass filter in CH_3CN under strictly anaerobic conditions results in the release of NO· to give acetonitrile-bound $[Fe^{II}(N3PyS)(CH_3CN)]BF_4$ (**1**). The rebinding of NO· was shown to be reversible for several cycles.[63] However, photoirradiation under aerobic conditions leads to the immediate disappearance of **2** (λ = 350, 450, 550 nm) and formation of a spectrum with λ = 415, 450, and 490 nm, which is reminiscent of $[Fe^{II}(N3PyS)(CH_3CN)]BF_4$ (**1**). This spectrum rapidly decays (60 s) to form a new species with an intense peak at 840 nm (ε = 1700 M^{-1} cm^{-1}) (Figure 5, top left). The 840 nm band persists for about 1 h at UV−vis concentrations (0.2 mM) and then slowly bleaches. This

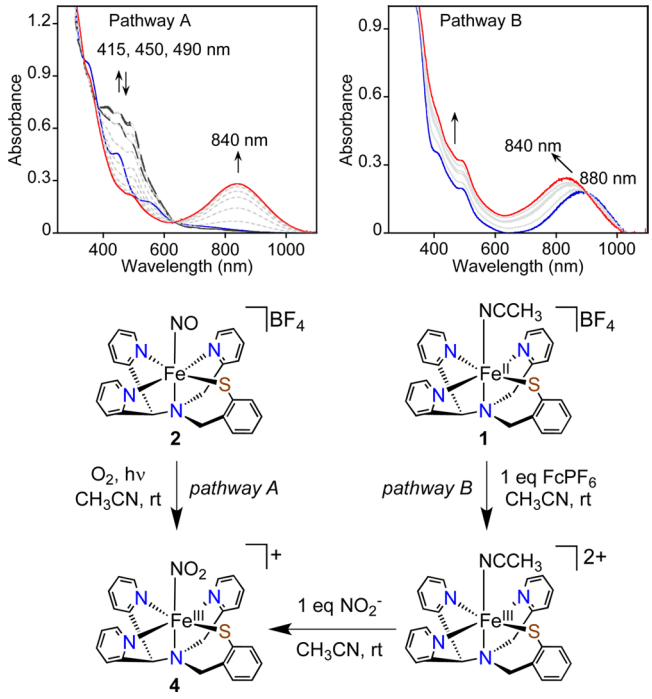

Figure 5. Top left: Time-resolved UV−vis spectra (0−10 min) showing the generation of $[Fe^{III}(NO_2)(N3PyS)]^+$ (**4**, red line) in CH_3CN by photoirradiation of $[Fe(NO)(N3PyS)]^+$ (**2**, dark blue line) in air. Initial spectra indicate generation of $[Fe^{II}(N3PyS)(CH_3CN)]BF_4$ (**1**) (λ = 415, 450, 490 nm, black, dashed). The subsequent spectra (light gray, dotted) display the decay of these bands with concomitant growth at 840 nm, with the final spectrum of **4** in red. Top right: Time-resolved UV−vis spectra (0−10 min) showing the generation of $[Fe^{III}(NO_2)(N3PyS)]^+$ (**4**, red line) in CH_3CN by addition of 1 equiv of Bu_4NNO_2 after *in situ* generation of $[Fe^{III}(N3PyS)]^{2+}$ (**1** + $[FeCp_2]^+$, dark blue line). Bottom: Generation of $[Fe^{III}(NO_2)(N3PyS)]^+$ (**4**) via two different pathways.

decomposition occurs more rapidly at higher concentrations, as observed in FTIR, EPR, and CSI-MS experiments (see below). Control experiments with **2** exposed to O_2 in the dark leads only to very slow (>3 h) and incomplete formation of the 840 nm species. This new feature at λ = 840 nm is similar to that seen for six-coordinate iron(III)−nitrite complexes.[19] Initial efforts to identify the product involved an analytical method (QUANTOFIX semiquantitative test strips) for identifying the presence of nitrite (NO_2^-) in solution. For these experiments, the photoirradiation reaction was run in CH_2Cl_2 in order to allow for aqueous extraction of any nitrite product. Extraction from the reaction mixture with an aqueous NaCl solution led to the identification of NO_2^- as a reaction product in 33% yield. These results suggested that photoirradiation of **2** in the presence of O_2 leads to formation of the Fe^{III}−nitrite complex $[Fe^{III}(NO_2)(N3PyS)]^+$ (**4**).

Further evidence for the production of an Fe^{III}−nitrite complex comes from the independent synthesis shown in Figure 5, bottom, together with the photoirradiation pathway. Addition of 1 equiv of the one-electron oxidant $FcPF_6$ to **1** in CH_3CN under anaerobic conditions leads to a color change to brown-green and a new band with λ_{max} = 880 nm (Figure S2). This species can be assigned to the one-electron oxidized $[Fe^{III}(N3PyS)]^{2+}$ (supported by EPR spectroscopy and CSI-MS, vide infra). Subsequent addition of 1 equiv of Bu_4NNO_2 resulted in a shift from 880 to 840 nm, consistent with the generation of $[Fe^{III}(NO_2)(N3PyS)]^+$ and matching the

DOI: 10.1021/jacs.5b12741
J. Am. Chem. Soc. 2016, 138, 3107−3117

spectrum seen for the aerobic photoirradiation pathway for the {FeNO}^{7} complex (Figure 5, top right).

Infrared Spectroscopy. Characterization of an Iron(III)−Nitrite Complex. The product of the reaction of {FeNO}^{7} complex **2** with O_2 in CH_3CN was monitored by transmittance FTIR and sample illumination with the 514 nm emission from an argon laser (100 mW illumination for 10 s). "Dark" minus "illuminated" difference spectra show positive bands at 1649 and 1737 cm^{-1}, which correspond to the loss of the ν(NO) bands of the low-spin {FeNO}^{7} and high-spin {FeNO}^{7} states of **2** prepared with unlabeled NO· (Figure 6),

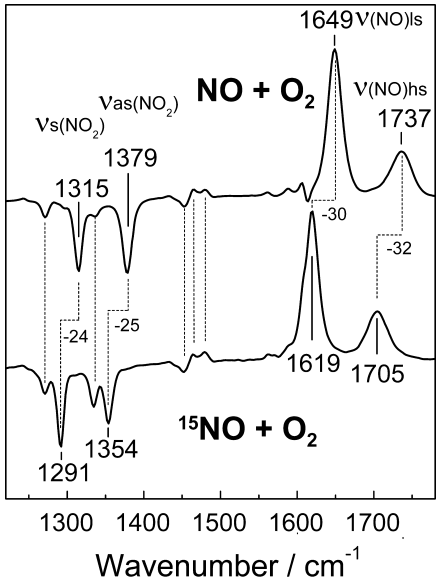

Figure 6. Room-temperature "dark" minus "illuminated" FTIR difference spectra of **2** in O_2-saturated CD_3CN (top trace, unlabeled NO·; bottom trace, ^{15}NO·).

while two negative bands at 1315 and 1379 cm^{-1} are consistent with $\nu_s(NO_2)$ and $\nu_{as}(NO_2)$ from an iron(III)−nitro complex based on their fundamental frequencies and isotope sensitivity.[70,71] Reacting **2**-^{15}**NO** with O_2 results in downshifts of the $\nu_s(NO_2)$ and $\nu_{as}(NO_2)$ modes to 1291 (−24) and 1354 (−25) cm^{-1}, respectively. Other weaker differential signals are assigned to N3PyS ligand vibrations affected by the oxidation of the nitrosyl group to nitrite. Evidence of intensity borrowing between the N3PyS ligand vibrations and ^{15}N-nitro vibrations is also observed in the 1300 cm^{-1} region.

The origin of the two oxygen atoms in the nitrite product was further analyzed by FTIR using ^{18}O-labeling. Using the doubly labeled **2**-^{15}**N**^{18}**O** results in downshifts of the ν(NO) and $\nu(NO_2)$ modes that match well with the calculated frequencies expected for a 2 AMU gain, and addition of $^{18}O_2$ to **2**-^{15}**N**^{18}**O** results in further downshifts of the $\nu(NO_2)$ modes (Figure 7). Due to vibrational mixing between the $\nu(NO_2)$ modes and weak N3PyS ligand vibrations in the 1300 cm^{-1} region, peak frequencies of individual bands do not provide a direct determination of the isotope shifts of the fundamental $\nu(NO_2)$ modes. Nevertheless, it is important to note that the reactions of **2**-^{15}**N**^{18}**O** + $^{16}O_2$ and **2**-^{15}**N**^{16}**O** + $^{18}O_2$ show the same set of bands in the $\nu(NO_2)$ region of the FTIR difference spectra. Thus, despite complication from vibrational coupling of the $\nu(NO_2)$ modes with N3PyS ligand vibrations, the FTIR data demonstrate that the O atom of the NO group is retained in the nitrite product. Indeed, without strict retention of the O

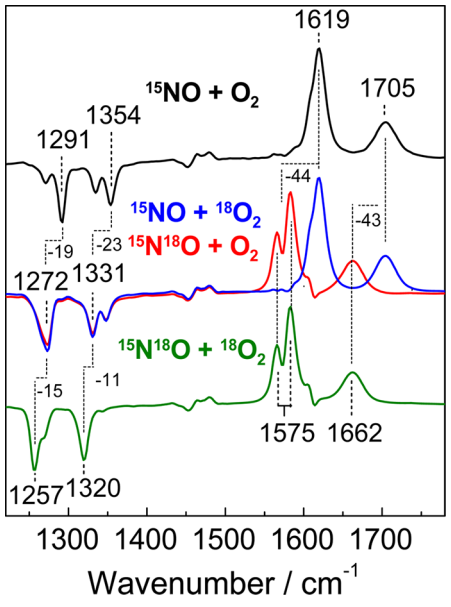

Figure 7. Room-temperature "dark" minus "illuminated" FTIR difference spectra of **2** in CD_3CN (top trace, ^{15}NO· reaction with $^{16}O_2$; middle traces are the results of different ^{16}O- vs ^{18}O-atom compositions; bottom trace, $^{15}N^{18}$O· reaction with $^{18}O_2$).

atom from NO·, the combined 1/3 vs 2/3 ^{18}O atom composition of the starting reactants should result in different ^{18}O-enrichment in the nitrite product and different FTIR signals in the 1300 cm^{-1} region.

Cryospray Ionization Mass Spectrometry (CSI-MS). Analysis of the reaction of **2** with O_2 under photoirradiation in CH_3CN by low-temperature, high-resolution electrospray (or cryospray) ionization mass spectrometry provided further insights into the formation and decay of the $Fe^{III}(NO_2^-)$ complex. A sample of **2** under aerobic conditions was photoirradiated with a 150 W xenon lamp (λ > 400 nm), and the reaction mixture was analyzed by CSI-MS over a 10 min period. As seen in Figure 8, the base peak is centered at

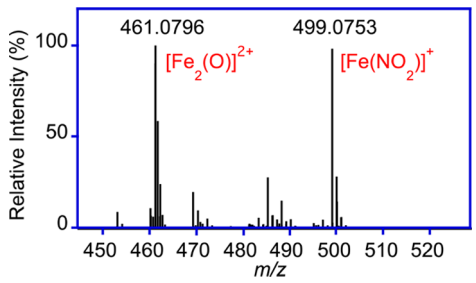

Figure 8. Mass spectrum of a sample of [Fe(NO)(N3PyS)]BF_4 (**2**) in CH_3CN after 10 min of photoirradiation (150 W xenon lamp: λ > 400 nm) in air.

m/z 499.0753, corresponding to the anticipated nitrite complex $[Fe^{III}(NO_2)(N3PyS)]^+$ and exhibiting the theoretically predicted isotope pattern (see Supporting Information). The other major species that appears at m/z 461.0796 is consistent with a diferric, oxo-bridged complex with formula $[(Fe^{III}(N3PyS))_2O]^{2+}$, which can be seen as a side product in the MS experiments with high complex concentration. Other minor products grow in over time and correspond to mono- and dioxygenated species of formulas $[Fe^{II}(N3PyS(O))]^+$ (m/z

DOI: 10.1021/jacs.5b12741
J. Am. Chem. Soc. 2016, 138, 3107−3117

469.0770) and $[Fe^{II}(N3PyS(O)_2)]^+$ (m/z 485.0724), respectively (see Supporting Information). Tandem MS/MS measurements using $^{18}O_2$ (see below) support their assignment as ligand modified S-oxygenates, as opposed to iron oxygenates. A small amount of five-coordinate species $[Fe^{II}(N3PyS)]^+$ (m/z 453.0821) is also observed.

The $Fe^{III}(NO_2^-)$ complex **4** was generated chemically via pathway B (Figure 5, bottom) and characterized by CSI-MS for comparison (Figure S5). Upon oxidation of $[Fe^{II}(N3PyS)]^+$ (**1**, m/z 453.0838) by $[FeCp_2]BF_4$ in CH_3CN, a new species is observed (m/z 247.0552) corresponding to the one-electron oxidized $[Fe^{III}(N3PyS)(CH_3CN)]^{2+}$. Addition of Bu_4NNO_2 affords a new base peak at m/z 499.0783, which is the same base peak seen in the photolytic aerobic oxidation of **2**, corresponding to **4**. Monitoring the reaction mixture over a 20 min period revealed the decay of the peak corresponding to **4** and the growth of peaks at m/z 485.0737, 483.0813, and 461.0832 which correspond to $[Fe^{II}(N3PySO_2)]^+$, $[Fe(NO)(N3PyS)]^+$, and $[(Fe^{III}(N3PyS))_2O]^{2+}$, respectively. The formation of the dimer species likely results from the one-electron oxidized $[Fe^{III}(N3PyS)(CH_3CN)]^{2+}$ that interacts with some trace moisture in the system. The two other species arise from decay pathways for complex **4**, which could include nitrite reduction and O atom transfer to the sulfur donor to give S-oxygenated products. Isotope labeling experiments were performed to provide further insight into the mechanism of formation and decay of **4**.

Isotope Labeling. Reaction of **2** with excess $^{18}O_2$ (saturated in CH_3CN) under the same photoirradiation conditions as mentioned above yielded a peak at m/z 501.0823, which grows in over a 25 min period, while the relative intensity of the peak for the starting material $[Fe(NO)(N3PyS)]^+$ (m/z 483.0832) decreases (Figure 9).

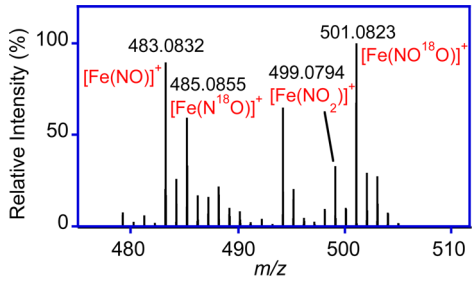

Figure 9. CSI-MS of the reaction of **2** + $^{18}O_2$ (saturated in CH_3CN) obtained after 25 min of photoirradiation.

The new peak (and isotope pattern) at 501.0823 can be assigned to $[Fe(N^{16}O)(N3PyS)+^{18}O]^+$, in which one O atom from $^{18}O_2$ has been incorporated into the complex. This product could correspond to either the expected Fe^{III}–nitrite complex **4** or an S-oxygenated Fe(NO) complex. Tandem MS/MS experiments on the 501.0823 peak showed that both species are present, with a fragmentation pattern consistent with the loss of NO_2·, as well as loss of NO· and retention of one O atom in the ligand (Figure S8). In addition to the peak at 501.0823, there is a relatively intense peak at m/z 485.0855 that corresponds to an $Fe(N^{18}O)$ complex (confirmed by MS/MS). The presence of this species is consistent with nitrite reduction via O atom transfer from the mixed label $Fe(N^{16}O^{18}O)$ complex to a S donor of another molecule through an intermolecular mechanism. A low intensity peak at m/z 499.0794 is also observed corresponding to $[Fe(N^{16}O)(N3PyS)+^{16}O]^+$, which can result from nitrite reduction and transfer of ^{16}O to the S donor of an $Fe(N^{16}O)$ complex. Analogous oxygen atom transfer from nitrite to biologically relevant thiols (cysteine and glutathione), which resulted in the sulfenic acids CysS(O)H and GS(O)H, was reported to be mediated by water-soluble ferriheme models.[26,72]

EPR Spectroscopy. The X-band EPR spectrum of the reaction of **2**/light/O_2 is shown in Figure 10. The spectrum

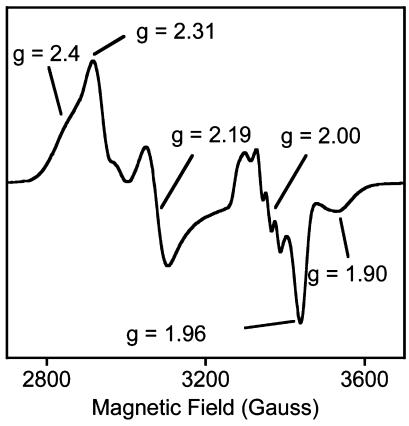

Figure 10. EPR spectrum (12 K, 1.8 mM in toluene/CH_3CN) of $[Fe^{III}(NO_2)(N3PyS)]^+$ (**4**) generated via pathway A.

reveals evidence for three species, including two low-spin iron(III) species and a spectrum that matches the $\{FeNO\}^7$ complex **2**. The Fe^{III} species can be seen in two rhombic low-spin signals, one with g = 2.31, 2.19, and 1.96, and the other with g = 2.4 (shoulder), 2.19, and 1.90. The more narrow signal centered at g = 2.00 is consistent with the $\{FeNO\}^7$ complex **2**, exhibiting well-resolved hyperfine coupling from the nitrogen atom of the NO ligand. The broader rhombic Fe^{III} signals are consistent with previously characterized nonheme low-spin $Fe^{III}(NO_2^-)$ complexes[21,22] and may represent different conformers of the $Fe^{III}(NO_2^-)$ complex or byproducts of the oxidation reaction and nitrite complex decomposition. The presence of the $\{FeNO\}^7$ complex in the EPR spectrum is consistent with the relatively rapid decay of the iron(III)–nitrite complex at higher concentrations to regenerate the $\{FeNO\}^7$ complex along with S-oxygenated products, as shown in the CSI-MS analysis as well as the EPR spectrum of **4** generated via pathway B from Figure 5. The production of the $Fe(NO_2^-)$ complex **4** by chemical oxidation of **1** followed by addition of Bu_4NNO_2 gives rise to a similar EPR spectrum, with rhombic low-spin Fe^{III} signals that can be assigned to **4**, and the hyperfine split spectrum centered at g = 2.00 coming from $\{FeNO\}^7$ (Figure S12). These data confirm the +3 oxidation state of the nitrite complex and are consistent with its decay, through O atom transfer to sulfur, to give the $\{FeNO\}^7$ complex.

Mechanism. The FTIR and CSI-MS studies with isotopically labeled O_2 indicate that only one O atom from O_2 is incorporated into NO_2^- and led to the proposed mechanism in Scheme 1. Photoirradiation of complex **2** results in the release of NO· to give a five-coordinate Fe^{II} complex, providing an open coordination site on the iron(II) for O_2 binding and generation of an Fe^{III}-superoxo transient species. Rebound of the free NO· with the $Fe^{III}(O_2^-)$ species can form an O-bound Fe-peroxynitrite (Fe-PN) intermediate. Linkage isomerization to a N-bound peroxynitrito species $[Fe^{III}–N(O)OO]^+$ may

DOI: 10.1021/jacs.5b12741
J. Am. Chem. Soc. 2016, 138, 3107–3117

Scheme 1. Proposed Mechanism for the Photoinitiated Production of $[Fe^{III}(NO_2)(N3PyS)]^+$ from $[Fe(NO)(N3PyS)]^+$ and Dioxygen

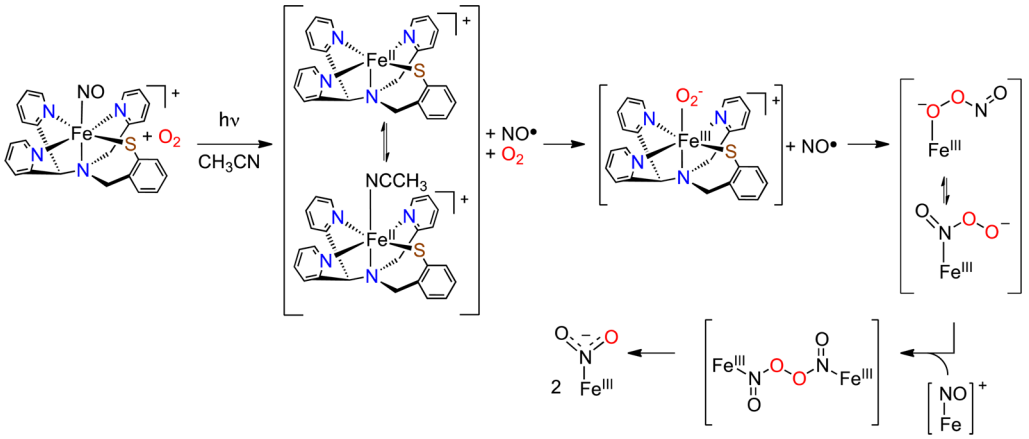

occur before reaction with a second $\{FeNO\}^7$ complex, giving rise to a PN-bridging diiron species that can undergo O–O bond cleavage, yielding $Fe^{III}(NO_2)$. This mechanism leads to incorporation of only one ^{18}O label in the final nitrite product. The direct reaction of O_2 with 2 NO· molecules to give NO_2· was considered, but this is a third-order reaction,[73,74] and since the NO· concentration is expected to remain low, the formation of NO_2· will be kinetically much less favorable than the binding of O_2 to five-coordinate Fe^{II} to generate Fe^{III}-superoxo before rebound of NO·.

The proposed mechanism has precedent in metal-nitrosyl chemistry. A Cr–NO complex[35] has been shown to undergo laser flash photolysis in an O_2-saturated solution to give a proposed $Cr–O_2^-$ species, similar to the first step in Scheme 1. The $Cr–O_2^-$ species then reacts with the released NO· to give a putative chromium–peroxynitrite intermediate ($[Cr^{III}–OONO]^{2+}$), which then undergoes a net isomerization to give a nitrato-chromium(III) species. Further precedence comes from a report on a Rh–NO complex, which undergoes Rh–NO photolysis to give a $Rh–O_2^-$ intermediate in the presence of O_2, which yields a $Rh–NO_3^-$ product.[75] Finally, Re–NO and Co–NO complexes are also known to react with O_2 to give metal–nitrite ($M–NO_2^-$) complexes.[32,38]

Trapping Experiments. To obtain further evidence for the proposed Fe-superoxo intermediate shown in Scheme 1, efforts were made to intercept this species by the addition of thiophenol as an external sulfur substrate. The Fe–NO complex **2** was exposed to O_2 and light in the presence of 1.5 equiv of thiophenol, and the spectrum for **2** initially converted to the CH_3CN-bound $[Fe^{II}(N3PyS)(CH_3CN)]BF_4$ (**1**, λ = 415, 450, 490 nm). The bands corresponding to **1** then decay with concomitant growth of the 840 nm band corresponding to **4** (Figure 11). Analysis by ^1H NMR showed that PhSH was oxidized to diphenyl disulfide. These results are consistent with PhSH intercepting the proposed Fe^{III}-superoxo intermediate, initially inhibiting the formation of **4**, followed by the production of **4** once the PhSH has been depleted.

A modified mechanism incorporating the oxidation of thiophenol is shown in Scheme 2. The superoxo-iron(III) species is intercepted by a thiophenol substrate, resulting in production of diphenyl disulfide and **1**. The disulfide product could come from H atom abstraction by $Fe^{III}(O_2^-)$, or possibly O atom transfer to give a transient sulfenic acid product (PhS(O)H), which is likely not stable and may react with

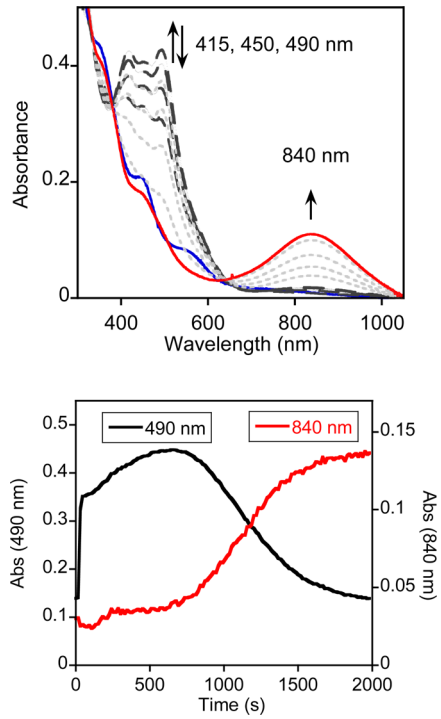

Figure 11. UV–vis spectral analysis (top) of the photoirradiation of $[Fe(NO)(N3PyS)]BF_4$ (**2**) (dark blue line) in air in the presence of thiophenol (1.5 equiv). Early time points (black, dashed) are consistent with the formation of $[Fe^{II}(N3PyS)(CH_3CN)]BF_4$ (**1**) (95% yield) via photodissociation of NO·, followed by the decay of this species and generation of $[Fe^{III}(NO_2)(N3PyS)]^+$ (**4**) (light gray, dotted) until maximal absorbance is reached (red). Change in absorbance of the peaks at 490 and 840 nm versus time (bottom). The decay of **1** and the growth of **4** begin at ~700 s.

additional PhSH to give PhS–SPh and H_2O.[72] Upon oxidation of all of the PhSH, the $Fe^{III}(O_2^-)$ complex then reacts with NO· and yields the nitrite product.

S-Oxygenation versus Nitric Oxide Oxidation. Solvent Effects. As previously reported, $[Fe^{II}(N3PyS)(solv)]^+$ (**1**) reacts rapidly with O_2 in methanol to give a S-oxygenated sulfinato-iron(II) complex.[62] This reaction proceeds through an initial green species (674 nm), which yields X-ray quality crystals of the $[Fe^{II}(N3PySO_2)(NCS)]$ complex following addition of the NCS^- anion. When the $\{FeNO\}^7$ complex **2**

DOI: 10.1021/jacs.5b12741
J. Am. Chem. Soc. 2016, 138, 3107–3117

Scheme 2. Proposed Reaction Pathway for the Aerobic Photoirradiation of [Fe(NO)(N3PyS)]$^+$ in the Presence of Thiophenol

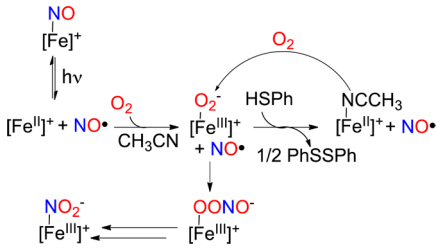

is photolyzed in methanol and exposed to O_2, the same green species (λ = 674 nm) corresponding to the S-oxygenation pathway is formed, with no evidence of the $Fe^{III}(NO_2^-)$ complex (840 nm) that is selectively produced in CH_3CN (Figure 12). In the absence of photolysis, the reaction of **2** and

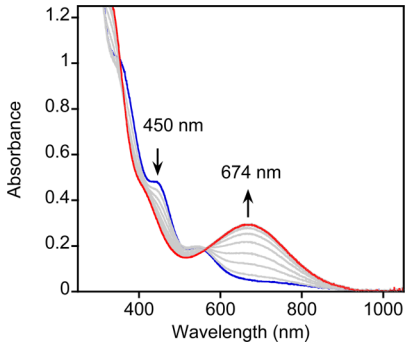

Figure 12. Time-resolved UV−vis spectra (0−30 min) showing the generation of the green species (674 nm) by aerobic photoirradiation of [Fe(NO)(N3PyS)]BF_4 (**2**) in CH_3OH.

O_2 in CH_3OH is much slower (>3 h) and incomplete. If the aerobic photoirradiation of **2** is run in a mixed solvent (10% MeOH in MeCN), a shoulder corresponding to the 674 nm band is observed together with the band assigned to the $Fe^{III}(NO_2)$ product (840 nm) (Figure 13).

Analysis of the reaction of **2** + O_2 under photoirradiation in MeOH by CSI-MS is consistent with the UV−vis data. Before irradiation, an intense peak corresponding to the starting material [Fe(NO)(N3PyS)]$^+$ (**2**, m/z 483.0813) is observed,

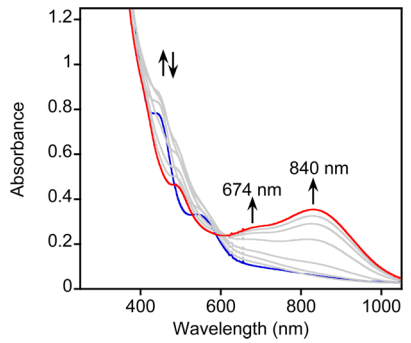

Figure 13. Time-resolved UV−vis spectra (0−10 min) showing the mixture of products upon aerobic irradiation of [Fe(NO)(N3PyS)]-BF_4 (**2**) in 10% CH_3OH (in CH_3CN), where the 840 nm band corresponds to $[Fe^{III}(NO_2)(N3PyS)]^+$ and the 674 nm band corresponds to S-oxygenation.

along with a second peak that can be assigned to $[Fe^{III}(OCH_3)(N3PyS)]^+$ (m/z 484.0975), which is likely a decomposition product from the aerobic conditions of the electrospray (Figure S13). The peak for **2** disappears within 5 min of photoirradiation, and the formation of $[Fe^{III}(OCH_3)(N3PyS + O)]^+$ (m/z 500.0963) is observed as the dominant species. After 10 min of photoirradiation, the further oxidized products $[Fe^{III}(OCH_3)(N3PyS + 2O)]^+$ and $[Fe^{III}(OCH_3)(N3PyS + 3O)]^+$ are observed, consistent with additional S-oxygenation. The mass spectral data, therefore, show only formation of S-oxygenated products $[Fe^{III}(OCH_3)(N3PySO_{1-3})]^+$, and not the Fe^{III}-nitrite species **4** in MeOH (Figure S14).

These results suggest that upon Fe−NO cleavage in **2** induced by visible light, S-oxygenation proceeds faster than NO· oxygenation in CH_3OH, whereas in CH_3CN, the formation of the Fe^{III}-nitrite complex is favored (Scheme 3).

Scheme 3. Proposed Solvent Effect on the Fate of the Iron(III)-Superoxo Intermediate in the Aerobic Photoirradiation of 2

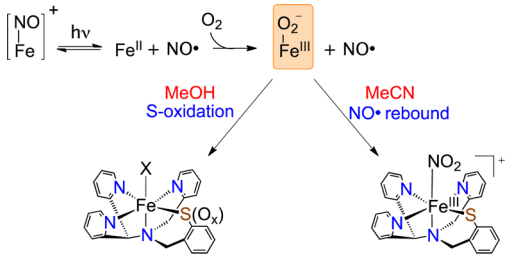

It should be noted that the anaerobic photolysis of **2** in CH_3OH behaves similarly to that in CH_3CN,[63] revealing only the reversible cleavage of the Fe−NO bond by UV−vis spectroscopy (Figure S15). The results obtained under aerobic conditions are consistent with the formation of a common Fe^{III}-superoxo intermediate in both CH_3CN and MeOH for $[Fe^{II}(N3PyS)]^+$, which then diverges to S-oxygenation or NO· rebound depending upon the solvent. We suggest that, in a protic solvent such as CH_3OH, the $Fe^{III}(O_2^-)$ species may protonate or H-bond with solvent and become a more reactive oxidant, which is then immediately reduced by sulfur, the most accessible reductant. In aprotic CH_3CN, the superoxo species may have a longer lifetime, which favors the NO· rebound pathway.

CONCLUSIONS

Spectroscopic and structural assignments have shown that the $\{FeNO\}^7$ complex [Fe(NO)(N3PyS)]BF_4 (**2**) exhibits rare spin-crossover behavior for an iron-nitrosyl species. A low-spin, S = 1/2 ground state is observed at 0−150 K, but upon warming to higher temperatures, a high-spin, S = 3/2 state is populated. This complex is also photolabile, releasing NO· upon irradiation, and was employed to show that photoactivation of a nonheme $\{FeNO\}^7$ can provide controlled access to Fe/O_2 reactivity. Much work has gone into designing nonheme iron complexes that will bind and react with O_2, and the results presented here suggest that light-triggered release of NO· may be a good strategy for future targeting of O_2 activation by nonheme iron complexes. Irradiating [Fe(NO)-(N3PyS)]BF_4 with visible light creates an open site at the iron center, providing a pathway for formation of a putative Fe^{III}-superoxo intermediate that can rapidly recombine with the

DOI: 10.1021/jacs.5b12741
J. Am. Chem. Soc. 2016, 138, 3107−3117

photolyzed NO· to give $[Fe^{III}(NO_2)(N3PyS)]^+$ (**4**), as confirmed by FTIR, CSI-MS, EPR, and UV−vis spectroscopy. Trapping experiments and isotope labeling studies are consistent with both Fe^{III}-superoxo and Fe^{III}-peroxynitrite intermediates being generated along the path to the Fe^{III}−NO_2 complex. The dramatic solvent dependence for the reactivity of the thiolate-ligated $\{FeNO\}^7$ complex with O_2 in visible light can be explained by the stability of the proposed Fe^{III}−O_2^- intermediate being highly dependent on its local environment, yielding sulfur oxygenated products in protic solvents but an Fe^{III}−nitrite complex in aprotic solvents. Finally, we have shown that a coordinated thiolate ligand can undergo S-oxygenation by the Fe^{III}−nitrite complex **4**, providing a novel example of NiR reactivity with a thiolate-ligated nonheme iron center. In summary, this work provides a rare example of NOD-like activity by a nonheme iron complex and suggests that nonheme iron-containing proteins could play a role in the scavenging of NO· in aerobic organisms while at the same time providing a new pathway for biological nitrite reduction (NiR activity) using metal-bound thiolates as the reducing agents.

■ ASSOCIATED CONTENT

Supporting Information

The Supporting Information is available free of charge on the ACS Publications website at DOI: 10.1021/jacs.5b12741.

X-ray experimental details, CSI-MS, EPR, and UV−vis spectroscopy (PDF)

Crystallographic data for **2** (CIF)

■ AUTHOR INFORMATION

Corresponding Authors

*dpg@jhu.edu

*moennelo@ohsu.edu

*ivana.ivanovic-burmazovic@fau.de

Present Address

#Department of Life Science, Faculty and Graduate School of Engineering and Resource Science, Akita University, Akita 010-8502, Japan.

Notes

The authors declare no competing financial interest.

■ ACKNOWLEDGMENTS

The NIH (GM62309 and GM101153 to D.P.G. and GM74785 to P.M.L.) is gratefully acknowledged for financial support. I.I.-B. and M.D. gratefully acknowledge support through the "Solar Technologies Go Hybrid" initiative of the State of Bavaria.

■ REFERENCES

(1) Fukuto, J. M.; Cisneros, C. J.; Kinkade, R. L. *J. Inorg. Biochem.* **2013**, *118*, 201.

(2) Ignarro, L. J.; Cirino, G.; Casini, A.; Napoli, C. *J. Cardiovasc. Pharmacol.* **1999**, *34*, 879.

(3) Moncada, S.; Palmer, R. M. J.; Higgs, E. A. *Pharmacol. Rev.* **1991**, *43*, 109.

(4) *Nitric Oxide: Biology and Pathobiology*; Ignarro, L. J., Ed.; Academic Press: San Diego, 2000.

(5) Munro, O. Q.; Scheidt, W. R. *Inorg. Chem.* **1998**, *37*, 2308.

(6) Hibbs, J. B.; Taintor, R. R.; Vavrin, Z. *Science* **1987**, *235*, 473.

(7) Iyengar, R.; Stuehr, D. J.; Marletta, M. A. *Proc. Natl. Acad. Sci. U. S. A.* **1987**, *84*, 6369.

(8) Bueno, M.; Wang, J.; Mora, A. L.; Gladwin, M. T. *Antioxid. Redox Signaling* **2013**, *18*, 1797.

(9) Gladwin, M. T.; Grubina, R.; Doyle, M. P. *Acc. Chem. Res.* **2009**, *42*, 157.

(10) Shiva, S.; Wang, X.; Ringwood, L. A.; Xu, X. Y.; Yuditskaya, S.; Annavajjhala, V.; Miyajima, H.; Hogg, N.; Harris, Z. L.; Gladwin, M. T. *Nat. Chem. Biol.* **2006**, *2*, 486.

(11) Cosby, K.; Partovi, K. S.; Crawford, J. H.; Patel, R. P.; Reiter, C. D.; Martyr, S.; Yang, B. K.; Waclawiw, M. A.; Zalos, G.; Xu, X. L.; Huang, K. T.; Shields, H.; Kim-Shapiro, D. B.; Schechter, A. N.; Cannon, R. O.; Gladwin, M. T. *Nat. Med.* **2003**, *9*, 1498.

(12) Maia, L. B.; Moura, J. J. G. *Chem. Rev.* **2014**, *114*, 5273.

(13) Kevil, C. G.; Kolluru, G. K.; Pattillo, C. B.; Giordano, T. *Free Radical Biol. Med.* **2011**, *51*, 576.

(14) Heinecke, J.; Ford, P. C. *Coord. Chem. Rev.* **2010**, *254*, 235.

(15) Nagababu, E.; Ramasamy, S.; Rifkind, J. M. *Biochemistry* **2007**, *46*, 11650.

(16) Perissinotti, L. L.; Marti, M. A.; Doctorovich, F.; Luque, F. J.; Estrin, D. A. *Biochemistry* **2008**, *47*, 9793.

(17) Ford, P. C.; Lorkovic, I. M. *Chem. Rev.* **2002**, *102*, 993.

(18) Miljkovic, J. L.; Kenkel, I.; Ivanović-Burmazović, I.; Filipovic, M. R. *Angew. Chem., Int. Ed.* **2013**, *52*, 12061.

(19) Afshar, R. K.; Eroy-Reveles, A. A.; Olmstead, M. M.; Mascharak, P. K. *Inorg. Chem.* **2006**, *45*, 10347.

(20) Cheng, L.; Powell, D. R.; Khan, M. A.; Richter-Addo, G. B. *Chem. Commun.* **2000**, 2301.

(21) Patra, A. K.; Afshar, R. K.; Rowland, J. M.; Olmstead, M. M.; Mascharak, P. K. *Angew. Chem., Int. Ed.* **2003**, *42*, 4517.

(22) Villar-Acevedo, G.; Nam, E.; Fitch, S.; Benedict, J.; Freudenthal, J.; Kaminsky, W.; Kovacs, J. A. *J. Am. Chem. Soc.* **2011**, *133*, 1419.

(23) Hematian, S.; Kenkel, I.; Shubina, T. E.; Dürr, M.; Liu, J. J.; Siegler, M. A.; Ivanović-Burmazović, I.; Karlin, K. D. *J. Am. Chem. Soc.* **2015**, *137*, 6602.

(24) Weber, B.; Görls, H.; Rudolph, M.; Jäger, E.-G. *Inorg. Chim. Acta* **2002**, *337*, 247.

(25) Heinecke, J. L.; Khin, C.; Pereira, J. C. M.; Suarez, S. A.; Iretskii, A. V.; Doctorovich, F.; Ford, P. C. *J. Am. Chem. Soc.* **2013**, *135*, 4007.

(26) Khin, C.; Heinecke, J.; Ford, P. C. *J. Am. Chem. Soc.* **2008**, *130*, 13830.

(27) Matson, E. M.; Park, Y. J.; Fout, A. R. *J. Am. Chem. Soc.* **2014**, *136*, 17398.

(28) Tsou, C.-C.; Yang, W.-L.; Liaw, W.-F. *J. Am. Chem. Soc.* **2013**, *135*, 18758.

(29) Schopfer, M. P.; Wang, J.; Karlin, K. D. *Inorg. Chem.* **2010**, *49*, 6267.

(30) Gunaydin, H.; Houk, K. N. *Chem. Res. Toxicol.* **2009**, *22*, 894.

(31) Herold, S.; Koppenol, W. H. *Coord. Chem. Rev.* **2005**, *249*, 499.

(32) Frech, C. M.; Blacque, O.; Schmalle, H. W.; Berke, H. *Dalton Trans.* **2006**, 4590.

(33) Kim, S.; Siegler, M. A.; Karlin, K. D. *Chem. Commun.* **2014**, *50*, 2844.

(34) Maiti, D.; Lee, D.-H.; Sarjeant, A. A. N.; Pau, M. Y. M.; Solomon, E. I.; Gaoutchenova, K.; Sundermeyer, J.; Karlin, K. D. *J. Am. Chem. Soc.* **2008**, *130*, 6700.

(35) Nemes, A.; Pestovsky, O.; Bakac, A. *J. Am. Chem. Soc.* **2002**, *124*, 421.

(36) Park, G. Y.; Deepalatha, S.; Puiu, S. C.; Lee, D.-H.; Mondal, B.; Sarjeant, A. A. N.; del Rio, D.; Pau, M. Y. M.; Solomon, E. I.; Karlin, K. D. *JBIC, J. Biol. Inorg. Chem.* **2009**, *14*, 1301.

(37) Subedi, H.; Brasch, N. E. *Inorg. Chem.* **2013**, *52*, 11608.

(38) Thyagarajan, S.; Incarvito, C. D.; Rheingold, A. L.; Theopold, K. H. *Inorg. Chim. Acta* **2003**, *345*, 333.

(39) Yokoyama, A.; Cho, K.-B.; Karlin, K. D.; Nam, W. *J. Am. Chem. Soc.* **2013**, *135*, 14900.

(40) Skodje, K. M.; Williard, P. G.; Kim, E. *Dalton Trans.* **2012**, *41*, 7849.

(41) Tran, N. G.; Kalyvas, H.; Skodje, K. M.; Hayashi, T.; Moënne-Loccoz, P.; Callan, P. E.; Shearer, J.; Kirschenbaum, L. J.; Kim, E. *J. Am. Chem. Soc.* **2011**, *133*, 1184.

(42) McCleverty, J. A. *Chem. Rev.* **2004**, *104*, 403.

DOI: 10.1021/jacs.5b12741
J. Am. Chem. Soc. 2016, 138, 3107−3117

(43) Roncaroli, F.; Videla, M.; Slep, L. D.; Olabe, J. A. *Coord. Chem. Rev.* **2007**, *251*, 1903.
(44) Speelman, A. L.; Lehnert, N. *Acc. Chem. Res.* **2014**, *47*, 1106.
(45) Zheng, S.; Berto, T. C.; Dahl, E. W.; Hoffman, M. B.; Speelman, A. L.; Lehnert, N. *J. Am. Chem. Soc.* **2013**, *135*, 4902.
(46) Jiang, Y. B.; Hayashi, T.; Matsumura, H.; Do, L. H.; Majumdar, A.; Lippard, S. J.; Moënne-Loccoz, P. *J. Am. Chem. Soc.* **2014**, *136*, 12524.
(47) Berto, T. C.; Speelman, A. L.; Zheng, S.; Lehnert, N. *Coord. Chem. Rev.* **2013**, *257*, 244.
(48) Yeung, N.; Lin, Y. W.; Gao, Y. G.; Zhao, X.; Russell, B. S.; Lei, L. Y.; Miner, K. D.; Robinson, H.; Lu, Y. *Nature* **2009**, *462*, 1079.
(49) Sanders, B. C.; Hassan, S. M.; Harrop, T. C. *J. Am. Chem. Soc.* **2014**, *136*, 10230.
(50) Gardner, P. R. *J. Inorg. Biochem.* **2005**, *99*, 247.
(51) Gardner, P. R.; Gardner, A. M.; Martin, L. A.; Salzman, A. L. *Proc. Natl. Acad. Sci. U. S. A.* **1998**, *95*, 10378.
(52) Clarkson, S. G.; Basolo, F. *Inorg. Chem.* **1973**, *12*, 1528.
(53) Frangione, M.; Port, J.; Baldiwala, M.; Judd, A.; Galley, J.; DeVega, M.; Linna, K.; Caron, L.; Anderson, E.; Goodwin, J. A. *Inorg. Chem.* **1997**, *36*, 1904.
(54) Yokoyama, A.; Han, J. E.; Cho, J.; Kubo, M.; Ogura, T.; Siegler, M. A.; Karlin, K. D.; Nam, W. *J. Am. Chem. Soc.* **2012**, *134*, 15269.
(55) Yokoyama, A.; Han, J. E.; Karlin, K. D.; Nam, W. *Chem. Commun.* **2014**, *50*, 1742.
(56) Badiei, Y. M.; Siegler, M. A.; Goldberg, D. P. *J. Am. Chem. Soc.* **2011**, *133*, 1274.
(57) Cho, J.; Woo, J.; Nam, W. *J. Am. Chem. Soc.* **2012**, *134*, 11112.
(58) Jiang, Y. B.; Widger, L. R.; Kasper, G. D.; Siegler, M. A.; Goldberg, D. P. *J. Am. Chem. Soc.* **2010**, *132*, 12214.
(59) Sallmann, M.; Siewert, I.; Fohlmeister, L.; Limberg, C.; Knispel, C. *Angew. Chem., Int. Ed.* **2012**, *51*, 2234.
(60) Gonzalez-Ovalle, L. E.; Quesne, M. G.; Kumar, D.; Goldberg, D. P.; de Visser, S. P. *Org. Biomol. Chem.* **2012**, *10*, 5401.
(61) Kumar, D.; Sastry, G. N.; Goldberg, D. P.; de Visser, S. P. *J. Phys. Chem. A* **2012**, *116*, 582.
(62) McQuilken, A. C.; Jiang, Y. B.; Siegler, M. A.; Goldberg, D. P. *J. Am. Chem. Soc.* **2012**, *134*, 8758.
(63) McQuilken, A. C.; Ha, Y.; Sutherlin, K. D.; Siegler, M. A.; Hodgson, K. O.; Hedman, B.; Solomon, E. I.; Jameson, G. N. L.; Goldberg, D. P. *J. Am. Chem. Soc.* **2013**, *135*, 14024.
(64) Gardner, J. D.; Pierce, B. S.; Fox, B. G.; Brunold, T. C. *Biochemistry* **2010**, *49*, 6033.
(65) Tchesnokov, E. P.; Wilbanks, S. M.; Jameson, G. N. L. *Biochemistry* **2012**, *51*, 257.
(66) Li, J.; Banerjee, A.; Pawlak, P. L.; Brennessel, W. W.; Chavez, F. A. *Inorg. Chem.* **2014**, *53*, 5414.
(67) Li, M.; Bonnet, D.; Bill, E.; Neese, F.; Weyhermüller, T.; Blum, N.; Sellmann, D.; Wieghardt, K. *Inorg. Chem.* **2002**, *41*, 3444.
(68) Schopfer, M. P.; Mondal, B.; Lee, D. H.; Sarjeant, A. A. N.; Karlin, K. D. *J. Am. Chem. Soc.* **2009**, *131*, 11304.
(69) Conradie, J.; Quarless, D. A.; Hsu, H.-F.; Harrop, T. C.; Lippard, S. J.; Koch, S. A.; Ghosh, A. *J. Am. Chem. Soc.* **2007**, *129*, 10446.
(70) Kurtikyan, T. S.; Martirosyan, G. G.; Lorkovic, I. M.; Ford, P. C. *J. Am. Chem. Soc.* **2002**, *124*, 10124.
(71) Nakamoto, K. *Infrared and Raman Spectroscopy of Inorganic and Coordination Compounds*, 5th ed.; John Wiley and Sons, Inc.: New York, 1997; Vols. *A, B*.
(72) Heinecke, J.; Ford, P. C. *J. Am. Chem. Soc.* **2010**, *132*, 9240.
(73) Goldstein, S.; Czapski, G. *J. Am. Chem. Soc.* **1995**, *117*, 12078.
(74) Nottingham, W. C.; Sutter, J. R. *Int. J. Chem. Kinet.* **1986**, *18*, 1289.
(75) Song, W.; Kristian, K. E.; Bakac, A. *Chem. - Eur. J.* **2011**, *17*, 4513.

DOI: 10.1021/jacs.5b12741
J. Am. Chem. Soc. 2016, 138, 3107−3117